International Journal of Bifurcation and Chaos, Vol. 25, No. 3 (2015) 1550037 (14 pages)

DOI: 10.1142/S0218127415500376

A Low-Dimensional Principal Manifold as the "Attractor Backbone" of a Chaotic Beam System

Erik M. Bollt* and Joseph D. Skufca†
Department of Mathematics, Clarkson University,
Potsdam, NY 13676, USA
**bolltem@clarkson.edu*
†*jskufca@clarkson.edu*

Received December 31, 2013

We model an elastic beam subject to a contact load which displaces under a chaotic external forcing, motivated by application of a ship carrying either a crane, or fluids in internal tanks. This model not only has rich dynamics and relevance in its own right, it gives rise to a Partial Differential Equation (PDE) whose solutions are chaotic, with an attractor whose points lie "near" a low-dimensional curve. This form identifies a data-driven dimensionality reduction which encapsulates a Cartesian product, approximately, of a principal manifold, corresponding to spatial regularity, against a temporal complex dynamics of the intrinsic variable of the manifold. The principal manifold element serves to translate the complex information at one site to all other sites on the beam. Although points of the attractor do not lie on the principal manifold, they lie sufficiently close that we describe that manifold as a "backbone" running through the attractor, allowing the manifold to serve as a suitable space to approximate behaviors.

Keywords: Reduced order model; ROMS; principal curve; principal manifold; low dimensionality; dimension reduction.

1. Motivation

The strength of ships remains one of the most challenging problems of engineering design. These complex structures are both large and expensive, with obvious trade-offs of strength for weight, cost and speed. Of particular difficulty for the design and analysis of ships and ship-based structures is the dynamic load environment. Although the romantic image might be that the ship's strength is challenged by icebergs or rocks, the reality is that most large structural damage to ships results from the recurrent dynamic interaction with the waves or the resultant motion of cargo driven dynamically by wave action (to include free surface motion of fluid inside tanks). Recent examples such as structural problems on the Navy's Arleigh Burke-class destroyers indicate that despite modern design tools, these engineering challenges have not been satisfactorily resolved.

A key aspect to the difficulty of this problem is that a hostile sea environment is not simply *dynamic*, but (in some sense) *indeterminate*, with wave fields the results of nonlinear interactions in the environment. Even when seas are somewhat regular, the resultant action of cargo can result in chaotic forcing of structures (as, for example, results from ship-board cranes). It is within this motivating framework that we consider the motion of a structural beam driven by complex forcing. Our primary goal within this work is to show how data-driven methods can be used to construct reduced order models of these dynamic settings.

Our primary example of consideration will be a simple linear beam (represented using a one-dimensional PDE), but driven by a chaotic forcing function. Consistent with our motivation as described above, we assume that most ship structures should be expected to be operating under

normal conditions. With expected ship lifetimes of tens of years, it is reasonable to assume that the structural components should be operated within the bounds of small perturbations, such that a linear beam model is appropriate. The challenge of the problem arises from complex forcing. Our work will examine techniques to exploit the structure generated by the underlying chaotic attractor to yield efficient representations of the driven PDE.

2. Beam Model

To develop our model for the forced beam motion, we start from the standard Euler–Lagrange beam equation for an elastic beam, where we assume constant material properties. Let $w = w(z,t)$ represent the displacement of the beam at location z and time t, measured with respect to reference (unloaded) configuration. The governing equation for transverse motion is given by the PDE

$$EIw_{zzzz} + \mu w_{tt} + cw_t = q(z,t), \tag{1}$$

with E the elastic modulus, I the moment of inertia, μ the mass per unit length of the beam, c a damping coefficient, and $q(z,t)$ giving the time varying load, measured in units of force per unit length. We take the problem domain to be $z \in [0, L]$, and $t \in [0, \infty)$. For specificity, we study the problem of a simply supported (pinned) beam, yielding boundary conditions

$$\begin{aligned} w(0,t) = w(L,t) = 0, \\ w_{zz}(0,t) = w_{zz}(L,t) = 0. \end{aligned} \tag{2}$$

Our primary interest was to understand the application of reduced order methods to problems of interesting beam motions (with a goal of recovering reduced representations from data). Therefore, we desired complex beam motions. For beams modeled by the linear PDE of (1), complex motions require complex behavior to be associated to the load. As a "toy model" representation of such a loading, we assume that the load on the system is a point force F, with the location at which the force is applied (z_q) varying in time in a chaotic motion. Specifically,

$$q(z,t) = -F\delta(z - z_q), \tag{3}$$

where $\delta(\cdot)$ is the Dirac delta function. (See Fig. 1.) The position z_q is governed by the well known

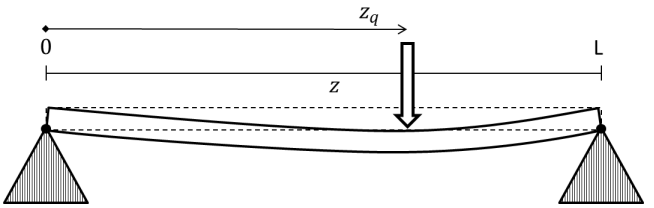

Fig. 1. Point load on a beam. The elastic beam, with simply supported ends, is loaded by a single point force whose position z_q is varying in time.

Duffing equation

$$\ddot{z}_d + \nu\dot{z}_d + \alpha z_d + \beta z_d^3 = \gamma\cos(\omega t), \tag{4}$$

where $z_d = z_d(t)$ is the state variable and $\nu, \alpha, \beta, \gamma$, and ω are scalar constants. The Duffing equation describes motion of a damped oscillator in a double well potential and is known to yield chaotic behavior for appropriate choice of parameter values. Because the Duffing equation gives behavior symmetric about the origin, we translate the Duffing coordinate by linear shift

$$z_q = z_d + \frac{L}{2}.$$

The resultant coupled system is given by

$$EIw_{zzzz} + \mu w_{tt} + cw_t = -F\delta(z - z_q), \tag{5a}$$

$$\ddot{z}_q + \nu\dot{z}_q + \alpha\left(z_q - \frac{L}{2}\right) + \beta\left(z_q - \frac{L}{2}\right)^3 = \gamma\cos(\omega t). \tag{5b}$$

We remark that a more typical model of chaotic forcing on a beam is to apply a load whose *amplitude* is varying in time. Here, we employ a fixed load, but with a chaotically varying point of attack. Our choice is driven by our application concept of a ship at sea, with point loads moving about the vessel, but we find the model sufficiently interesting, independent of that application.

2.1. *Numerical simulation*

To compute data associated for the beam motion, we use an implicit finite difference method for time-stepping of (5a) along with an explicit Runge–Kutta solver to compute solutions to (5b). We desire to numerically simulate the solution on a uniform spacial grid of $J + 1$ points, over the time interval

Table 1. Simulation parameters used throughout this article.

L	3.4
EI	200
μ	20
c	10
F	1
ν	0.02π
α	$-0.01\pi^2$
β	$0.01\pi^2$
γ	$0.003\pi^2$
ω	$\pi/10$

$[0, T]$. Discretizing time into N intervals, such that $\Delta t = T/N$, and defining $\Delta z = L/J$, we denote the approximate solution on this grid by

$$w_j^n \approx w(j\Delta z, n\Delta t), \tag{6}$$

$$z_q^n \approx z_q(n\Delta t), \quad j = 0, \ldots, J, \;\; n = 0, \ldots, N. \tag{7}$$

Throughout this note, our numerical simulations focus on the parameter set given in Table 1. The beam parameters were taken from an example problem in [Jin & Xing, 2007] and have no special significance other that being reasonable engineering values with some external source data that we could use for verification of our code, with the exception of damping coefficient c, which was selected *ad hoc*. The parameters for the Duffing equation are related to the classic parameter choice,[1] where we have simply used a time scaling to slow the forcing function to allow for better representation of the separation of time scales. However, we performed no search to find "interesting" parameter sets and we assume that the observed behaviors are (therefore) reasonably generic.

2.2. *Description of coupled system behavior*

In this section, we provide an explanation of the behaviors observed in the solution to (5) based on standard analysis approaches to such equations. We emphasize that the analysis is dependent upon a reasonably complete knowledge of the governing equations of the system. In Secs. 4–7 we describe techniques that allow for *discovery* of such structures from data, appropriate to typical real-world problems where system equations are not known. Our analysis is this section is meant to establish a framework that justifies the expectation that a manifold based approach to dimensionality reduction may be a fruitful approach to systems driven by complex forcing.

Starting from a realization that (5b) admits only numerical solutions, we may infer that standard analytic solutions to (5a) are not tractable. However, the standard approaches to the beam equation may still provide useful insight. In that direction, we first consider the associated homogeneous problem

$$EIw_{zzzz} + \mu w_{tt} + cw_t = 0.$$

If we assume that damping is small, we can reduce to the standard beam equation

$$EIw_{zzzz} + \mu w_{tt} = 0. \tag{8}$$

Under our assumed boundary condition of simply support ends, one easily shows that the eigenfunctions for the system are simply the Fourier modes given by

$$\phi_n = \sin\Big(\frac{n\pi z}{L}\Big),$$

with an associated Fourier series solution to (8). The inclusion of damping would not affect the identified modes, though it would affect the form of the series solution to the homogeneous problem.

Proceeding under the presumption that we have computed the homogeneous solution, the standard step in finding the most general solution would be to find a particular solution to (5a). However, because the forcing is time varying (and not known in closed form), we cannot proceed along that path. We can ignore that complexity if we consider the related problem

$$EIw_{zzzz} + \mu w_{tt} + cw_t = -F\delta(z - z^*), \tag{9}$$

where z^* denotes the *fixed* location of static point load on the beam. Because the right-hand side is time invariant, we can seek particular solutions that are not varying in time, of the form $w(z, t) = W_{z^*}(z)$, where this notation is meant to emphasize

[1] A classic choice of parameters for the Duffing equation is to take $\nu = 0.2, \alpha = -1, \beta = 1, \gamma = 0.3, \omega = 1$. We wanted to consider a load that moved more slowly, so we applied a change of time scales, such that time interval 2π under the classic Duffing representation would equate to 20 units of time for the beam problem.

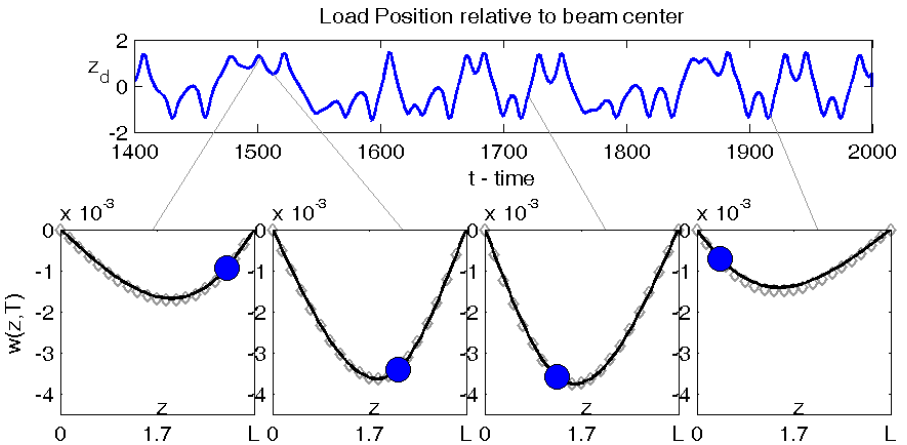

Fig. 2. Point load static approximation. (Upper) The position of the point load on the elastic beam. (Lower) Four snapshots (in time) of the numerical solution to (5) (black line). The blue dot shows the location of the load, while the diamonds give the approximation using the quasistatic solution (10).

that the solution is a function only of the spatial variable z, with a one parameter family of solutions to the family of problems specified to varying the location of the point load.

$$W_{z^*}(z) = \begin{cases} \dfrac{F(L-z^*)z^3 - z^*(L-z^*)z(2L-z^*)}{6LEI}, \\ \qquad\qquad 0 \le z \le z^* \\ \dfrac{F(L-z^*)z^3 - z^*(L-z^*)z(2L-z^*)}{6LEI} \\ \qquad -\dfrac{F(z-z^*)^3}{6EI}, \quad z^* < z \le L. \end{cases} \tag{10}$$

The usefulness of (10) is that if the repositioning of the load is sufficiently slow (with respect to beam dynamics) and if the vibrational energy in the beam is not too large, then solutions to (5a) can be approximately computed by simply knowing the location of the load:

$$w(z,t) \approx W_{z_q(t)}(z). \tag{11}$$

Figure 2 illustrates the reasonableness of this assumption by comparing the full numerical solution to the approximation computed using (11).

We refer to the solution given by (11) as the *quasistatic approximation*, where we use the more general interpretation of this term *quasistatic* to refer to forces varying slowly in time, with related analysis often associated with techniques of fast–slow system. Our approximation assumption is that the full solution at any instant in time does not vary far from the solution obtained by assuming that the load is not moving, ($\dot{z}_q \approx 0$), which is appropriate when $\dot{z}_q$ is small relative to the dynamics of the beam. We note that the quasistatic assumption ignores momentum of the beam, and we may expect larger errors to result from changing direction of motion of the load. Furthermore, we reemphasize that this approximation requires knowledge of the load position at any instant. Consequently, (11) should be viewed as an approximate solution to (5a), not to the full system (5).

Figure 3 further illustrates that the quasistatic approximation provides a reasonable representation of the ensemble of shapshots of the solution, where we consider all snapshots associated to a particular position of the load.

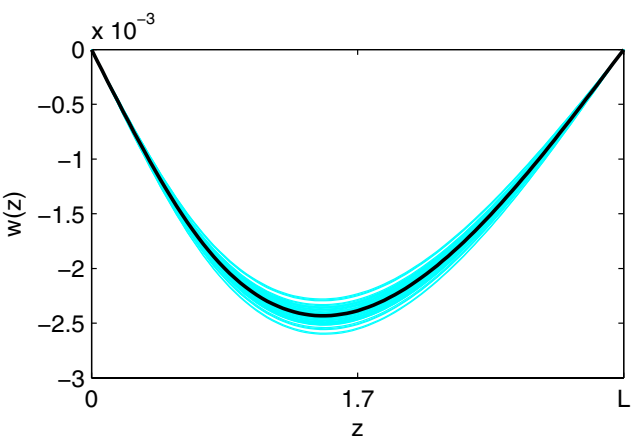

Fig. 3. Static approximation to ensemble. Taking $z^* = -1 + L/2$ we plot quasistatic solution (10) (black) against an ensemble of solutions snapshots taken at times where $z_q(t) = z^*$ (cyan).

Remark. Our key observation relevant to the above subsection is that the system appears to be "simple" in space while complex in time. If the load is not moving too quickly, then a closed form spatial description based on fixed load provides a good approximation to the dynamic problem. The chaotic behaviors in the dynamic problem are driven by the temporal complexity of the load movement. In the following sections, we show how this separability of behaviors can be (1) identified from data, and (2) exploited for the purpose of reduced order modeling.

3. Numerical Results, and Presentation in Delay Coordinates and Offset Coordinates

Consider simulations of the beam equations, Eq. (1). Because solutions are computed only on a grid, as described in Sec. 2.1, we focus on our solution computed on a spatial grid of 101 site locations, denoting solutions at each site by

$$w_j(t) := w(j\Delta z, t).$$

See Fig. 4, wherein a time series of a solution $w_{50}(t)$ near the center of the beam at site $j = 50$ is illustrated. Here we see an apparently classic view of a chaotic oscillation, and this pattern is repeated at other sites. See Fig. 5 for a full spatiotemporal view of a solution $w_j(t)$, $0 \le j \le 100$ for times $0 \le t \le 1000$. In this section, we will present solutions $w_j(t)$ both in time-delay coordinates and also in spatial offset coordinates. With these contrasting views, we begin to understand what apparently is an example of a chaotic attractor corresponding to temporal chaos, but with a great deal of spatial regularity.

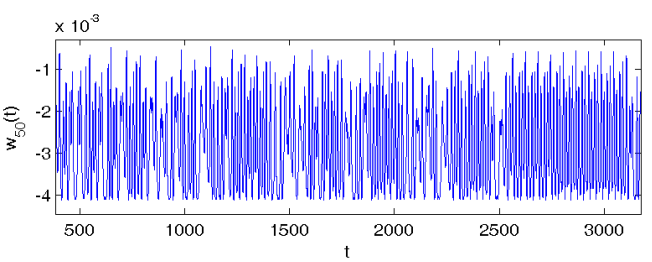

Fig. 4. A time series of a solution $w_{50}(t)$ of the beam, Eq. (1), at site $j = 50$ near the center of the simulated beam. Note the chaotic appearance of the oscillations at this "typical" site.

Time-delay embedding coordinates are now a classic method to understand low dimensionality present in a high-dimensional system. If the time-series has been generated by a "chaotic" dynamical system, data-only based analysis using the methods of embedding and attractor reconstruction, has become routine [Takens, 1981; Packard *et al.*, 1980; Eckmann & Ruelle, 1985; Kantz & Schreiber, 1997; Alligood *et al.*, 2000]. Suppose that an autonomous dynamical system,

$$\dot{x} = F(x), x(t) \in \Re^n, \quad \text{and} \quad x(t_0) = x_0, \quad (12)$$

has an invariant attractor. A nonautonomous system may also be placed into that framework by the usual method of augmenting the dimension to $n+1$, interpreting the time as a phase variable, allowing for recurrence by considering strobing. In general, the experimentalist who does not know the underlying global model Eq. (12) does not even know which are the correct variables to measure. Any single-channel data collected from the system can be considered to be from a scalar measurement function $h[x(t)] : \Re^n \to \Re$. Given a set of measurements $\{h[x(t_i)]\}_{i=0}^N$, taken at uniformly spaced times t_i, the method of time-delay embedding is to form the vector,

$$\mathbf{y}(t) = \langle h[x(t)], h[x(t-\tau)], h[x(t-2\tau)], \ldots, h[x(t-d\tau)]\rangle, \quad (13)$$

and one generally chooses τ to be some multiple of the sampling rate $\Delta t = t_{i+1} - t_i$. Takens [1981] proved that for topologically generic measurement function h, if the attractor A is a smooth m-dimensional manifold, then if one chooses the delay dimension to be $d \ge 2m + 1$, then Eq. (13) is an embedding, meaning there exists a one-to-one function $G : A \to \Re^d$, and G is a diffeomorphism. Sauer *et al.* [1991] proved an extension to allow for nonsmooth A, and even fractal A. Ott and Yorke [2003] established a Platonic version of Whitney embedding theorem which provides generic conditions under which a measurement function can provide an embedding. To reconstruct the attractor, both these results assume that the data is clean, and the data set is arbitrarily long. Neither assumption is physically realizable, but nonetheless, time-delay reconstruction has found many applications to nonlinear modeling and to prediction. See [Abarbenel *et al.*, 1993; Farmer & Sidorowich, 1988; Takens, 1981; Packard *et al.*, 1980; Eckmann & Ruelle, 1985; Kantz & Schreiber, 1997; Alligood *et al.*, 2000]. See

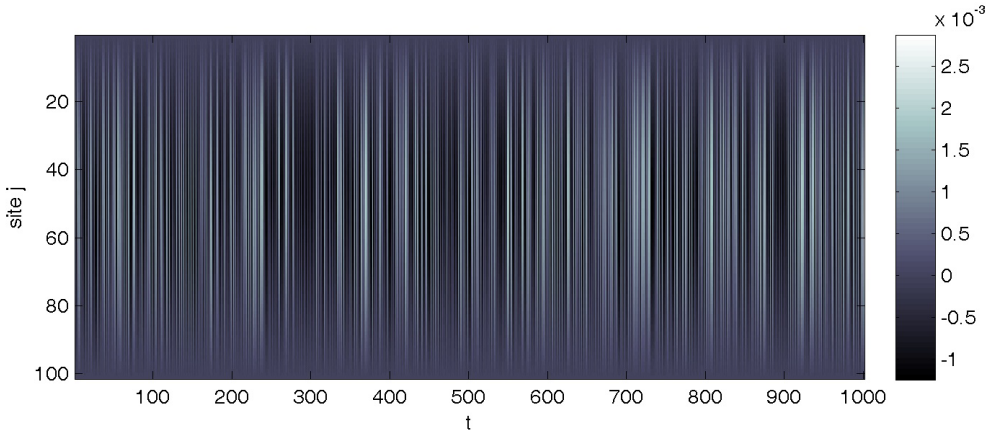

Fig. 5. A full spatiotemporal presentation $w_j(t)$ of a solution of the beam Eq. (1). Shade intensity shows the value of w for each site j on the beam at each time t. Comparing to Figs. 4, 6 and 8 we begin to infer that this dynamical system embodies temporal chaos but spatial order.

Fig. 6 as a two-dimensional view of an underlying chaotic attractor present in the beam system.

As alternative (and/or supplement) to time-delay embedding, we may also use the information from multiple sites to construct a coordinate representation. In choosing such representations, we need to understand to what degree solutions $w(z,t)$ and $w(z',t)$ at sites z and z' may correlate. To this end, first we demonstrate solutions at nearby sites and then at sites that are not nearby. See Fig. 8. That $w(z,t)$ and $w(z',t)$ lie roughly along a diagonal when $z \simeq z'$ is simply a reflection of continuity of solutions $w(z,t)$ with respect to z. More interestingly, even when z and z' are quite far apart, as shown in Fig. 8(b), the data lies on an apparently highly constrained set, which "suggests" a one-dimensional curve running through its center. Our reduced order modeling goal will be to *approximate* the system dynamics by restricting dynamics to that one-dimensional curve that runs through the data.

It is important here to emphasize that our intended reduced order model will not satisfy a convergence condition. The one-dimensional ansatz is

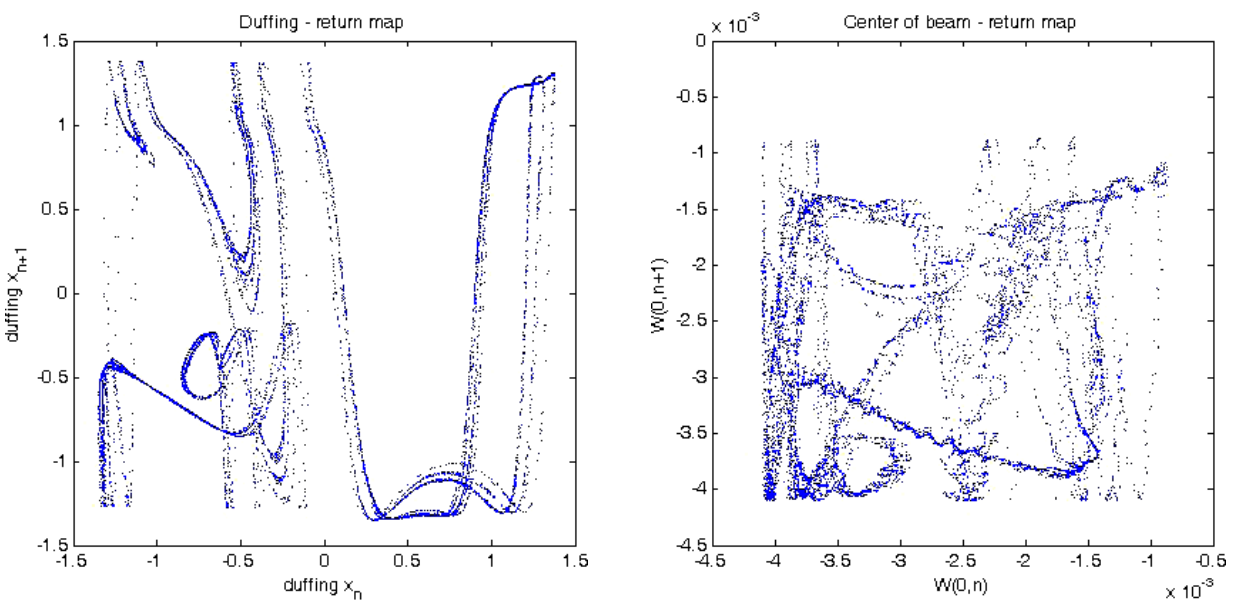

Fig. 6. A time-delay plot $(w(z,t), w(z,t-\tau))$ gives a time-delay embedding presentation for the beam Eq. (1), with parameters as in Fig. 4 suggesting a chaotic attractor, which reminds us of the chaotic attractor of a Duffing oscillator also shown in delay coordinates [Takens, 1981; Packard *et al.*, 1980; Eckmann & Ruelle, 1985; Kantz & Schreiber, 1997; Alligood *et al.*, 2000].

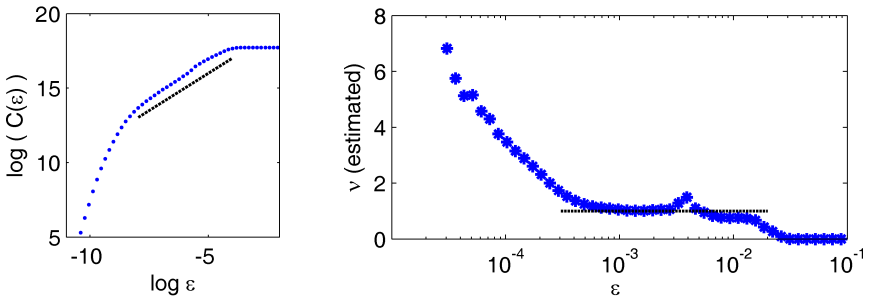

(a) (b)

Fig. 7. Correlation dimension estimates for the point cloud of data $\{w(t_n)\}$. (a) Log–log plot of correlation sum as a function of ϵ shows a linear scaling regime for intermediate values of ϵ. The dashed line illustrates a slope of 1. (b) Estimated dimension ν as a function of ϵ. At intermediate values, the estimate lies near $\nu \approx 1$, indicating a curve, while for small epsilon, the dimension continues to increase, indicating significant complexity (higher dimension) at small scales.

not a claim that the underlying system lies on a low-dimensional manifold. Rather, it argues only that the configurations are "close enough" to a one-dimensional manifold that the approximation can provide a useful model. We emphasize that we are presuming a data-driven modeling approach, and we use that data to more directly address this issue of how the existence of a low-dimensional "backbone" might be identified.

If we treat the $w(t) = [w_j(t)]$ as a vector in $J+1$ dimensional space (at each instant in time), then we may also view $\{w(t_n)\}_{n=0}^{N}$ as a cloud of points. As a typical approach, one could use the correlation dimension [Grassberger & Procaccia, 2007], as estimated using the correlation integral

$$C(\epsilon) = \lim_{k\to\infty} \frac{g}{k^2}, \tag{14}$$

where ϵ indicates a threshold distance, k is the number of considered points, and g is the total number of pairs of points within a distance ϵ. For small ϵ, the correlation integral should scale as

$$C(\epsilon) \sim \epsilon^{\nu}, \tag{15}$$

with ν the dimension of the underlying process that generated the data.

In Fig. 7, we show the results of applying this analysis to our dataset, computing both the correlation sum and then using that data to estimate dimension. We see that when ϵ is large, it covers the whole attractor, and the estimate is a zero-dimensional object. However, for mediate values of neighborhood size, the point-cloud appears to be approximately one-dimensional, with a clear linear scaling regime in the log–log plot of correlation sum.

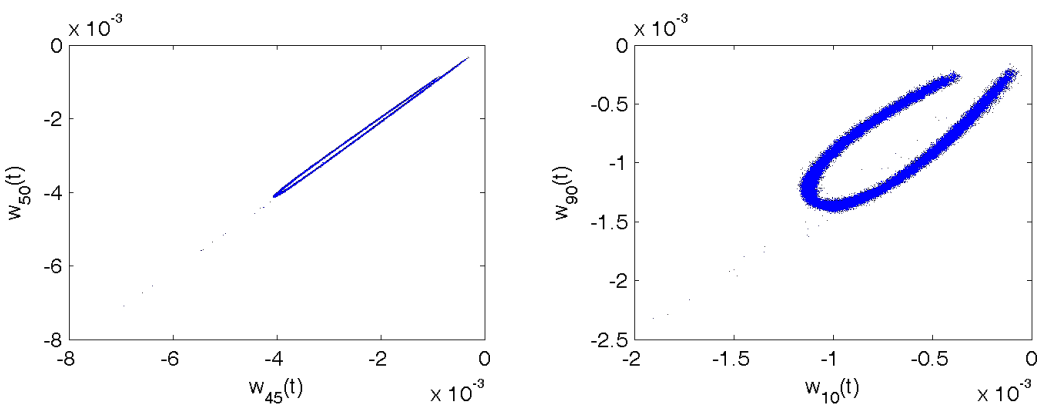

(a) (b)

Fig. 8. Spatial delays presentation $(w_j(t), w_{j'}(,t))$ at same times t, of beam data with parameters as in Fig. 4. (a) $j = 45$ and $j' = 50$, nearby sites. That the $(w_j(t), w_{j'}(,t))$ data lies near the diagonal at these two nearby sites $45 \simeq< 50$ agrees with a notion of continuity of the solutions $w(z,t)$ with respect to spatial displacement. Knowledge of one site solution allows approximate inference of the solution at the nearby site. (b) All the data at not-so nearby sites, $j = 10$, $j' = 90$, lies predominantly nearby a low-dimensional manifold, a curve. This strongly suggests that while the data may be temporally chaotic, it is spatially simple.

When ϵ is sufficiently small, the correlation integral captures the full detail of the attractor, which remains a high-dimensional object.

4. Approximating the Attractor

To develop our reduced order model, we take as *assumption* the existence of an attractor to the coupled system (5). The natural phase space for this system would be of the form $\mathcal{H} \times \mathcal{H} \times \mathbb{R}^2 \times \mathbb{R}$, where $\mathcal{H}$ is a function space of scalar valued functions over the interval $[0, L]$. A point in phase space gives beam displacement and beam velocity (each a function in $\mathcal{H}$) as well as the position and velocity of the load, with the final coordinate representing a time variable, as we require an extended phase space to represent the nonautonomous system. We may project this attractor onto the first component, where we seek to describe only the displacements of the beam, and denote the resultant set as $\mathcal{W} \subset \mathcal{H}$.

We presume that $\mathcal{W}$ retains a very rich, and high-dimensional structure. However, our *goal* is to provide a low-dimensional set that can "approximate" the attractor. Specifically, we seek smooth function

$$x : [0, L] \times [0, 1] \mapsto \mathbb{R} \quad (z, s) \mapsto x(z, s)$$

such that for any $w(\cdot) \in \mathcal{W}$ there exist an $s \in [0, 1]$ such that

$$\|w(\cdot) - x(\cdot, s)\|_H \leq r,$$

where $\|\cdot\|_H$ is a sup norm on the function space $\mathcal{H}$ and r is a small positive number. Implicit in this description is that $x(\cdot, s) \in \mathcal{H}$ for any fixed $s \in [0, 1]$. Then our reduced order *model of the attractor* is given by

$$\mathcal{A} = \{x(\cdot, s) \in \mathcal{H} \,|\, 0 \leq s \leq 1\}. \tag{16}$$

Heuristically, we would say that $\mathcal{A}$ *is an* r *approximation to* $\mathcal{W}$, but we will avoid the formalism of rigorously defining that statement. Additionally, we note that there are many such functions x that satisfy this condition, and our procedure simply builds one such instance. The key observation that results from (16) is that *the reduced order model approximates the dynamics as taking place on a finite length, one-dimensional curve in a function space.*

4.1. *Describing the attractor approximation*

Although not emphasized by the notation in (16), the attractor model is completely determined by the choice of function $x(z, s)$. Viewing this function as a surface over the two scalar input variables, we can describe that surface by defining "traces" $x(z^*, s), \quad 0 \leq s \leq 1$, where z^* is simply meant to indicate some fixed value of z.

Our discrete-based method is to define traces

$$x(z_j, s), \quad j = 1, \ldots, J-1, \quad z_j = j\delta z,$$

where we develop a trace at each of our spatial grid points. We denote these "skeleton" traces by

$$x_j(s) := x(z_j, s).$$

We use the method of *principal curves* to develop these traces, as described in Sec. 6. Given the collection of *skeleton traces*, we can describe the full surface by specifying that at any fixed $s = s^*$, determine $x(z, s^*)$ by cubic spline interpolation using knots

$$\{z_j, x_j(s^*)\}_j.$$

(Our choice of cubic spline is based on the physical problem, which should yield a continuous second derivative of beam shape as long as the load is finite.)

4.2. *Using the reduced order representation*

We note that a point in $\mathcal{A}$ describes a physical beam shape that should be "near" a shape allowed by the full attractor, such that points in $\mathcal{A}$ may be useful approximation to the real phase space. To define a point $\tilde{w}(\cdot) \in \mathcal{A}$, it is sufficient to identify the associated value s^* such that

$$\tilde{w}(\cdot) = x(\cdot, s^*). \tag{17}$$

This $\tilde{w}(\cdot)$ describes the "shape" of the beam. We note that "most" of the time, we can identify this shape by simply tracking the displacement of a single location on the beam. Suppose we know that at some instant, the displacement of the grid location j is some particular value w_j^*. Then

$$x_j(s) = w_j^*,$$

and (typically) the Implicit Function Theorem (IFT) yields

$$s^* = x_j^{-1}(w_j^*),$$

for appropriately defined inverse function. The full beam shape is given by (17). Because IFT may not hold at some particular points, we may occasionally

need another point, $x_k(s) = w_k^*$ to resolve s^*. Additionally, if we assume "noisy" measurements, then having information regarding beam displacement at more than one location could be used to formulate a maximum likelihood or Bayesian parameter estimation of s^*. We remark that "noise" can be viewed as the cumulative effect of errors in measurement along with the reality that $\mathcal{A}$ only approximates the full set of observable configurations, $\mathcal{W}$.

4.3. *Contrast with Karhunen–Loève modes*

An extremely popular method of modeling nonlinear dynamical systems is KL-method, [Kari, 1947; Loève, 1955, 1978], which is to develop time-averaged optimal modes using the so-called POD modes [Lumley, 1970; Holmes *et al.*, 1996; Sirovich, 1987], for a given observed data set, and then to perform a Galerkin projection to these modes. We acknowledge that this tool has been successfully employed against a vast multitude of problems, both linear and nonlinear. Our intent in this section is not to argue superiority of our method or even to qualitatively or quantitatively compare the two methods. Rather, we simply seek to clearly describe the difference between these data representations.

The objective of identifying POD modes is to allow for solutions $u(x,t)$ representations of the form

$$u(x,t) = \sum_n a_n(t)\psi_n(x), \tag{18}$$

where ψ_n represent a time-averaged optimal basis. The $a_n(t)$ give time varying amplitudes for the modes, and the solutions are determined by linear combination (superposition) of these discrete modes. In contrast to the KL representation of the data, we develop a representation which could be described as a continuous one parameter family of "modes," where each "mode" describes the solution, *without* superposition. Whereas dynamics in the KL framework is a system of ODEs describing the evolution of the amplitude with time, the dynamics in our framework would dictate the evolution of the intrinsic variable (or variable*s*), $s(t)$.

5. Background: Parameterized Coordinates in a Manifold Representation

A general topological manifold can be described as a topological space that on a small enough scale resembles the Euclidean space of a specific dimension, called the dimension of the manifold. We will take a manifold to be a subset of a q-dimensional Euclidean space such that open sets are homeomorphic ("looks like") in a p-dimensional Euclidean subspace, $p \leq q$ [Whitney, 1936]. Additionally we will take here a common interpretation of the phrase to mean a differentiable manifold, including the notion of an atlas of transition maps. Respecting this idea, to embed a point x from q-dimensional Euclidean space, into "intrinsic" variables y of a p-dimensional manifold, means that we can represent the manifold in terms of a vectorized parameterization,

$$\Phi : \mathbf{Y} \mapsto X, \tag{19}$$

where

$$\begin{aligned} x &= \Phi(y) \\ &= \langle \phi_1(y_1, y_2, \ldots, y_p), \phi_2(y_1, y_2, \ldots, y_p), \ldots, \\ &\quad \phi_q(y_1, y_2, \ldots, y_p) \rangle. \end{aligned} \tag{20}$$

Reviewing some familiar examples,

- The familiar $p = 1$ dimensional helix is parameterized by,
$$\begin{aligned} x &= \langle \phi_1(y), \phi_2(y), \phi_3(y) \rangle \\ &= \langle r\cos(y), r\sin(y), cy \rangle, \quad y \in \mathbb{R}, \\ &\qquad \text{and real constants, } r, c, \end{aligned} \tag{21}$$
to represent the $q = 3$ coordinates of ambient space $\mathbb{R}^3$.
- Similarly, the sphere is represented,
$$\begin{aligned} x &= \langle \phi_1(y_1, y_2), \phi_2(y_1, y_2), \phi_3(y_1, y_2) \rangle \\ &= \langle r\sin(y_1)\cos(y_2), r\sin(y_1)\sin(y_2), r\cos(y_1) \rangle, \\ &\quad y \in [0, 2\pi) \times [0, \pi) \subset \mathbb{R}^2, \\ &\qquad \text{and real constant, } r, \end{aligned} \tag{22}$$
and $y_1, y_2 \in \mathbb{R}$, is a $p = 2$ dimensional parameterization of each point on the manifold in $q = 3$ dimensional ambient space.

These intrinsic y-variables can be interpreted as directions to any point on the manifold relative to a base point on the manifold. Approximating high-dimensional X by lower-dimensional Y is what we mean by "data-reduction". We identify "reduced order modeling" to be the reduction of *dynamics* to intrinsic variables, which generally provides a simplification of the system.

6. Principal Curves and Principal Manifolds

We will adapt a tool from statistics called principal curves, and its generalization, principal manifolds to describe the behavior of a dynamical system evolving in high dimensions by a smooth manifold of much lower dimensionality, as suggested in Sec. 5. While principal curves have found many data processing applications from speech recognition [Kegl & Krzyzak, 2002], medicine [Reinhard & Niranjan, 1999], and physics [Friedsam & Oren, 1989], we will develop this area for use in a scenario where the dynamics evolve on a stable submanifold. Considering data points sampled from the invariant measure of a dynamical system as an orbit evolves, whose ω-limit set may not be smooth, we may nonetheless expect the data to reside stably near a smooth manifold. This sampled data set from an invariant measure may admit a statistical summary by a *principal manifold*.

Hastie & Stuetzle [1989] have defined a *principal curve* as a smooth one-dimensional curve that passes through the "middle" of a p-dimensional data set, $\{x_i\}_{i=1}^N \subset \Re^q$. From [Hastie & Stuetzle, 1989], in terms of a probability distribution of a random variable $X \in \Re^q$, with density h and finite second moment, from which data x is sampled, assume without loss of generality that $E(X) = 0$. A C^∞-smooth nonself intersecting curve is sought,

$$\Phi(y) = \langle \phi_1(y), \phi_2(y), \ldots, \phi_q(y) \rangle, \tag{23}$$

in $\Phi(y) \subset R^q$ over a closed subset $y \subset \Re^1$. A curve that "runs through the middle" of the data is described as "self-consistent" to define a principal curve [Hastie & Stuetzle, 1989] if for distribution h there is a Φ such that,

$$\Phi(\lambda) = E(X \,|\, \lambda_\Phi(X) = \lambda), \tag{24}$$

for a.e. λ. The "projection index" $\lambda_\Phi(x)$ for a data point x may be defined,

$$\lambda_\Phi(x) = \sup_\lambda \left\{ \lambda : \|x - \Phi(\lambda)\| = \inf_\mu \|x - \Phi(\mu)\| \right\}. \tag{25}$$

As depicted in Fig. 9, the idea of self-consistency is that each point of the curve should be the mean projection of the observations x' onto Φ around the point.

There are several different variations on this original definition [Hastie & Stuetzle, 1989] as reviewed in [Biau & Fischer, 2012], including constrained principal curves [Kegl *et al.*, 2000], bounded length [Biau & Fischer, 2012], or bounded turn [Sandilya & Kulkarni, 2002], and a semiparametric variation [Tibshirani, 1992], and principal oriented points [Delicado, 2001], to name a few directions of development to cope with various prior expectations of the data set and biases.

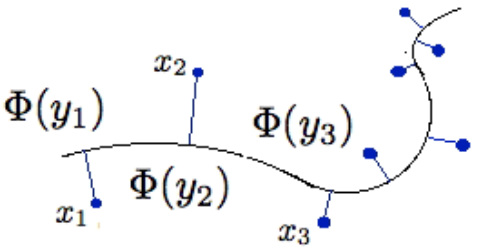

Fig. 9. Projection index to a principal curve. Figure inspired by [Biau & Fischer, 2012], the projection index $\lambda_\Phi(x)$ as the term appears in self-consistency definition Eqs. (24)–(25). Given a data point x_i, then the index i also indexes the parameterization y_i which stands for $t_\Phi(x_i)$.

7. Estimating a Principal Curve for a Beam Data Set

The main idea we wish to emphasize here when modeling high-dimensional data from dynamical systems is a *smooth* manifold through the data set. As such, we will adapt a standard cubic smoothing spline to the parametric setting which allows us to explicitly control the degree of smoothness trade-off with the degree we wish the curve to agree with the data. Cubic smoothing splines were similarly used in [Hastie & Stuetzle, 1989], and [Bollt, 2007]. Consider a list of scalar valued ordered pairs, $(s_i, W_i), i = 1, \ldots, N$, which we seek to model by the relationship $W_i = x(s_i)$. Then a cubic smoothing spline is a minimizer of the functional,

$$E(x) = p \sum_{i=1}^{n} |W_i - x(s_i)|^2 + (1-p) \int \lambda(s) |D^2 x(s)| ds, \tag{26}$$

where smoothing parameter $0 \leq p \leq 1$ allows us to choose an appropriate balance between minimizing model error at the data and minimizing the "roughness" of the model. There is a detailed literature [Boor, 1994] on the numerical analysis of this problem, but here we avoid such discussions and simply employ the robust solver algorithm built into the Matlab spline toolbox, called "csaps" [Matlab,

2010]. We extend the scalar nature of cubic smoothing spline by simply determining a set of splines, $\{x_j\}$, where x_j approximates the behavior at beam grid point j to model (approximate) Φ_j, the jth component function of Φ, from Eqs. (19) and (23).

The first step in developing a spline model is to develop a useful ordering of the data, as it is necessary to sort the data so that it best allows for a smooth curve to model the data. For the discussion here, we will take the beam displacements $w_j(t)$ at computed sites j and times t_n to be simply w_{jn}. Given the unstructured data set, $\{(t_n, w_{jn})\}_{n=0}^{N}$, for a fixed j, the plotted data will not suggest a smooth curve $x(s)$ because the *abscissa* of those data is temporal, while the manifold is a *spacial* structure. Points that are "nearby" in space (which should be used to estimate the local manifold behavior) need not be "nearby" in time. Therefore, a precursor step to apply a component-wise smoothing is to reindex the data to emphasize spatial continuity rather than temporal continuity. This is achieved simply by sorting such that following each $w_{j,n}$, the next data in the list is $w_{j,n'}$ which is closest in space.

This idea of "spatially close" warrants additional discussion. At time t_n, the displacement at each of the spatial grid points can be viewed as vector $W_{:,n}$, a point in $\mathbb{R}^{J+1}$. Finding nearest neighbors in a high-dimensional space can prove numerically challenging, both from an accuracy and time complexity standpoint. As such, we note that as we are making *a priori* assumption that the data lies near a one-dimensional curve, then a three-dimensional embedding should be sufficient to describe that curve. For computational ease (and because we expect it to be sufficient), we choose to determine spatial closeness by projecting the data onto $X := \mathbb{R}^3$, where our projection simply selects the $j = 10$, $j = 50$, and $j = 90$ components, where the choice of these particular sites is somewhat arbitrary. We note that points that are close in the full space will be close in X, and the resultant ordering should be appropriate for reasonable solutions from the smoothing spline.

We summarize this sorting procedure with the following algorithmic description:

(1) Create data matrix W of size $J + 1 \times N + 1$, where each row associates to a grid location on the beam, and each column associates to a particular time. Denote columns of this matrix as $W_{:,n}$.
(2) Identify n such that $W_{:,n}$ is in an extreme end point in the space X. Denote this data column as $W'_{:,0}$ stored as a column in array W', while deleting that column of data from array W. Let counter $c = 1$.
(3) Perform an ϵ-range search to $W'_{:,c-1}$. That is, find those columns $\mathcal{W}$ subset of the remaining data set W which are within ϵ of $W'_{:,c-1}$ (as measured in projected space X). Remove this datum $\mathcal{W}$ from the current remaining W.
(4) Choose $W'_{:,c} \in \mathcal{W}$ as the extremum,
$$W'_{:,c} = \arg\min_{w \in \mathcal{W}} \|w - W'_{:,c-1}\|.$$
(5) Increment the counter $c \mapsto c + 1$.
(6) Repeat Step 3 until the list W is exhausted and W' is a data set of the same size as the original.
(7) Compute $x_j(s)$ as a cubic smoothing spline fitted to data set $\{(\frac{i}{N}, W'_{j,i})\}_{i=0}^{c-1}$.

Note that generally W' will be a subset of the original set of points W, as $c - 1 \leq N$. The choice of ϵ in the range search is appropriately chosen as the cross-over scale, related to the correlation dimension, where the otherwise high-dimensional set takes on the characteristics of a low-dimensional set, in this case, one-dimensional.

Figure 10 illustrates the necessity of this algorithm, and the outcome of the above spatial sorting algorithm. We see the difference between a chaotic time series as seen when the data is sorted in time, and an "almost" smooth curve when sorted in space, ready for smoothing by a principal curve algorithm to produce $x(s)$, as is our goal here. In Fig. 11 we illustrate a few of the fitted curves $x_{10}(s)$, $x_{50}(s)$, and $x_{90}(s)$ through sorted data, $\{W'_{10,i}\}$, $\{W'_{50,i}\}$, $\{W'_{90,i}\}$, along with a projection of curves and data into a three-dimensional projection that emphasizes that curve $x(s)$ runs through the "center" of the data cloud.

7.1. *Validation of technique on beam data*

The goal of the methods described above is to develop a one-dimensional manifold that can approximate data on the attractor, where that approximation is data driven. Based on the assumed ansatz of a 1D curve, our approach is to lean on embedding theory and assume that tracking of only three beam locations should be sufficient to specify the parameter value s. We used this idea in

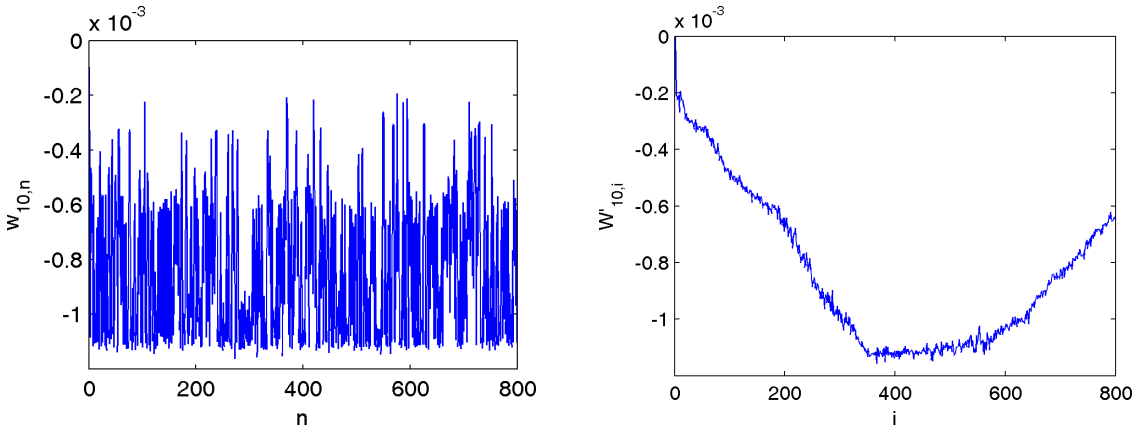

(a) (b)

Fig. 10. (a) The data $\{w_{j,n}\}_{n=0}^{N}$ at site $j = 10$, initially sorted as paced with time, and as a chaotic time series. (b) Sorted data $\{W'_{j,i}\}$ emphasize a "smoother" spatial curve as a pecursor step to a principal curve smoothing as illustrated in Fig. 11.

two ways:

- In constructing the smoothing splines, it is necessary for us to "reorder" the data before spline, where that reordering is meant to sequence the data based on nearness along the manifold as opposed to nearness in time. We use just three (arbitrarily chosen) locations ($j = 10, 50, 90$) to determine that ordering, significantly reducing the computational complexity.
- Once the spline structure is learned, to estimate the beam configuration, we need to know the value of intrinsic variable s. We determine s by knowing the location of the beam only at those three locations, and use that s to predict the beam displacement at all other sites.

Validation of these ideas is examined numerically, with the key results captured in Fig. 12. In Fig. 12(a), we show that the ordering determined at the three sites is sufficient to allow for smooth representation of the data at the other sites. The red curves represent the $x_j(s)$ drawn through the sorted data $\{W'_{j,i}\}$. Figure 12(b) illustrates how we may determine $s(t)$ by monitoring the position at only those three sites. We use $s(t)$ and the full set parameterization $x(s)$ to predict the position at *all* of the sites. In Fig. 12(c), we consider whether the monitoring of three sites is sufficient to estimate the data at all other sites, showing both the relative and absolute error at each site, averaged over the entire data set.

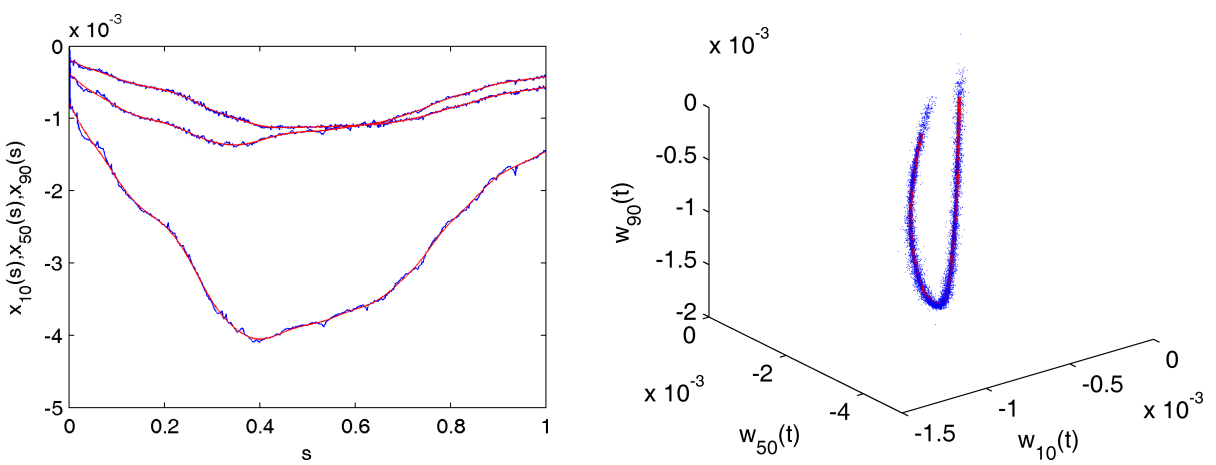

(a) (b)

Fig. 11. (a) Parameterized curves $x_j(s)$ (red) through sorted $\{W'_{j,i}\}_{i=0}^{N}$, at sites $j = 10, 50, 90$. (b) The modeled curves, $x_j(s)$ form a parameterized curve $x(s)$ (red) shown here in a three-dimensional representation, acting as a principal curve running through the middle of the data (blue dots).

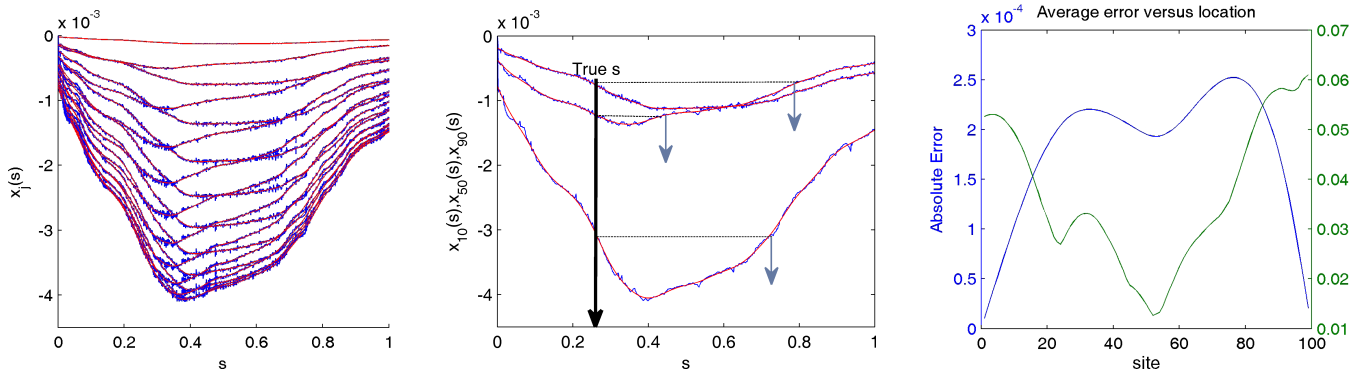

Fig. 12. Validation data. (a) The ordering determined using only sites $j = 10, 50, 90$ provides a reasonable reordering of the data at all other sites (blue) such that each can now be reasonably approximated by parameterized curves $x_j(s)$ (red). (b) Using measurements $w_j(t)$ at three locations allows for an unambiguous inversion of $x(s)$ to find $s(t)$. (c) Time average of absolute and relative error, observed over the entire data set, as a function of site (j).

As additional comments on validation, we note that the "error" described in Fig. 12 compares the data to the associated point on the 1D manifold that serves as a reduced order model of the attractor. As such, even if our numerical method gave an exact parameterization of the 1D curve, we still expect error, because *the real attractor is high dimensional and the points in configuration space do not lie on a 1D curve.* In other words, it is an error associated to reduced order modeling. Also, the method focuses on the solution representation based on knowledge of only a few locations (either measured from data or predicted from model). Modeling the dynamics (to predict parameter $s(t)$) is not the focus of this paper, but could be explored via time series analysis methods or (when data drive) by state observer methods.

8. Conclusions

In this work, we developed a new model of a chaotic beam inspired by a Naval application of bearing a load that may move upon the beam in an irregular way, such as a ship-board crane moving with pitch and roll of the ship or fluids moving within large tanks under free surface effect. We show that this dynamical system is relevant and rich in its own right. We also show that this model gives rise to an excellent paradigm for studying model reduction in a spatiotemporal system where one may hope to capture spatial regularity (approximating configurations as lying on a manifold) while retaining temporal complexity via the dynamics in the intrinsic variables of that manifold. As such, we demonstrate that a model of the manifold $x(s)$ can be developed as a stable principal curve which makes for practical translation of solutions from trusted solutions at position z on the beam to other positions z' understood as parameterization values s.

We describe this system as temporally chaotic but spatially regular. In some sense, this behavior is an expected outcome for a mechanical structure for which a great deal of regularity results from the continuity of physical parameters plus dissipation. Furthermore, while $x(s)$ developed for this model was that of a one-dimensional Lyapunov stable principal manifold running through the middle of the attractor, one dimensionality is, in some sense, due to the fact that the driving force on the beam is that of a single point contact. It could be expected that a higher-dimensional manifold would result from a more complex driving force. For example, a next level of complexity could be achieved by assuming two point masses moving on the beam, such as due to two cranes, or two tanks on board each containing moving fluids. Such a scenario would be expected to result in a two-dimensional principal manifold $x(s)$ which should be similarly Lyapunov stable to the corresponding higher-dimensional attractor, with a comparable spatially simple but temporally complex representation. Finally, we plan to pursue analytic confirmation of the stability of the attractor decomposition, and regularity analysis together with our dissipation explanation to confirm the reason behind the decomposition. We wish to close in pointing out a particularly useful aspect of the decomposition is that it yields a low-dimensional

model of the spatial structure together with a method that allows that the motion at one site can be a useful description and predictive representation of the system. The predictive model (for one site) may take the form of prior observations, a current mechanical experiment, or a low-dimensional ODE which has been parameter tuned as a state observer. This general framework will lead us in the near future to a parametric study of the system, where changing system parameters leads to a parameterized family of manifolds to model the attractor.

Acknowledgments

This work was supported by the Office of Naval Research under grant entitle, "Reduced-Order Representations for Design a Manifold Learning Approach to Reduced-Order Basis", under a BRC from the mathematics division.

References

Abarbenel, H., Brown, R., Sidorowich, J. & Tsimring, L. [1993] "The analysis of observed chaotic data in physical systems," *Rev. Mod. Phys.* **65**, 1331.

Alligood, T. K., Sauer, T. & Yorke, J. A. [2000] *Chaos: An Introduction to Dynamical Systems* (Springer).

Biau, G. & Fischer, A. [2012] "Parameter selection for principal curves," *IEEE Trans. Inform. Th.* **58**, 1924–1939.

Bollt, E. [2007] "Attractor modeling and empirical nonlinear model reduction of dissipative dynamical systems," *Int. J. Bifurcation and Chaos* **17**, 1199–1219.

Boor, C. D. [1994] *A Practical Guide to Splines* (Springer).

Delicado, P. [2001] "Another look at principal curves and surfaces, *J. Multivar. Anal.* **77**, 84116.

Eckmann, J. P. & Ruelle, D. [1985] "Ergodic theory of chaos and strange attractors," *Rev. Mod. Phys.* **57**, 617–656.

Farmer, J. & Sidorowich, J. [1988] "Exploiting chaos to predict the future and reduce noise," *Evolution, Learning, and Cognition* (World Scientific, Singapore), 277 pp.

Friedsam, H. & Oren, W. O. [1989] "The application of the principal curve analysis technique to smooth beamlines," *Proc. First Int. Workshop on Accelerator Alignment*, SLAC-OU13-11408.

Grassberger, P. & Procaccia, I. [2007] "Measuring the strangeness of strange attractors," *Physica D* **9**, 189–208.

Hastie, T. & Stuetzle, W. [1989] "Principal curves," *J. Amer. Statist. Assoc.* **84**, 502–516.

Holmes, P., Lumley, J. L. & Berkooz, G. [1996] *Turbulence, Coherent Structures, Dynamical Systems, and Symmetry* (Cambridge Press, NY).

Jin, J. Z. & Xing, J. T. [2007] "Transient dynamic analysis of a floating beam–water interaction system excited by the impact of a landing beam," *J. Sound Vibr.* **303**, 371–390.

Kantz, H. & Schreiber, T. [1997] *Nonlinear Time Series Analysis*, 2nd edition (Cambridge University Press, UK).

Kari, K. [1947] "über lineare Methoden in der Wahrscheinlichkeitsrechnung," *Ann. Acad. Sci. Fennicae. Ser. A. I. Math.-Phys.* **37**, 1–79.

Kegl, B., Krzyzak, A., Linder, T. & Zeger, K. [2000] "Learning and design of principal curves," *IEEE Trans. Patt. Anal. Mach. Intell.* **22**, 281–297.

Kegl, B. & Krzyzak, A. [2002] "Piecewise linear skeletonization using principal curves," *IEEE Trans. Patt. Anal. Mach. Intell.* **24**, 59–74.

Loève, M. [1955] *Probability Theory* (Van Nostrand, Princeton, NJ).

Loève, M. [1978] *Probability Theory*, Vol. II, 4th edition (Springer-Verlag).

Lumley, J. L. [1970] *Stochastic Tools in Turbulence* (Academic, NY).

Matlab [2010] 7.10.0.499 (R210a) with spline toolbox.

Ott, W. & Yorke, J. A. [2003] "Learning about reality from observation," *SIAM J. Appl. Dyn. Syst.* **2**, 297–322.

Packard, N., Crutchfield, J., Farmer, J. D. & Shaw, R. [1980] "Geometry from a time series," *Phys. Rev. Lett.* **45**, 712.

Reinhard, K. & Niranjan, M. [1999] "Parametric subspace modeling of speech transitions," *Speech Commun.* **27**, 19–42.

Sandilya, S. & Kulkarni, S. R. [2002] "Principal curves with bounded turn," *IEEE Trans. Inform. Th.* **48**, 2789–2793.

Sauer, T., Yorke, J. & Casdagli, M. [1991] "Embedology," *J. Stat. Phys.* **65**, 579–616.

Sirovich, L. [1987] "Turbulence and the dynamics of coherent structures. I — Coherent structures. II-Symmetries and transformations. III — Dynamics and scaling," *Quart. Appl. Math.* **45**, 561–571.

Takens, F. [1981] *Detecting Strange Attractors in Turbulence*, Lecture Notes in Mathematics (Springer-Verlag), 898 pp.

Tibshirani, R. [1992] "Principal curves revisited," *Statist. Comput.* **2**, 183–190.

Whitney, H. [1936] "Differentiable manifolds," *Ann. Math.* **37**, 645–680.